

# Polarization, Microscopic Origin, and Mode Structure of Luminescence and Lasing from Single ZnO Nanowires

H.-Y. Li,<sup>†</sup> S. Rühle,<sup>†</sup> R. Khedoe,<sup>†</sup> A. F. Koenderink,<sup>‡</sup> and D. Vanmaekelbergh<sup>\*,†</sup>

*Debye Institute for NanoMaterials Science, University of Utrecht, Princetonplein 5, 3508 TA Utrecht, The Netherlands, and Center for Nanophotonics, FOM Institute for Atomic and Molecular Physics (AMOLF), Science Park 104, NL-1098 XG, Amsterdam, The Netherlands*

Received May 29, 2009; Revised Manuscript Received August 15, 2009

## ABSTRACT

The emission spectrum of individual single crystalline ZnO nanowires shows three regimes characterized by distinct polarization properties and spatial emission patterns along the length of the wire. In the visible range below 2.9 eV, emission is polarized along the long axis of the wire, along the *c*-axis (*E*//*c*). In the second regime between 2.9 and 3.22 eV, Fabry-Pérot guided modes polarized perpendicular to the wire (*E*⊥*c*) prevail. From their dispersion, it is clear that these modes signify strong coupling between the B-exciton and linearly polarized transverse electric modes that are guided by the wire and trapped between the wire end facets. The third regime is characterized by uniform emission along the wire and a marked dip in the polarization at around the electronic band gap at 3.3 eV. Lasing is observed only in the second regime in which strong light-matter interaction prevails.

ZnO is one of the most attractive materials for optical applications in the visible and the near UV range, ranging from large-scale white-light illumination to miniaturized lasers for the near UV.<sup>1–5</sup> Furthermore, the unique properties of the semiconductor ZnO are of high interest in the field where advanced optics meets the nanoarea. Because of strong exciton transitions near the electronic band gap and an electron–hole binding energy of 60 meV, the optical properties are dominated by strong light-matter interaction, involving exciton polaritons.<sup>6–8</sup> In macroscopic ZnO structures, light absorption and emission mediated by exciton-polaritons has been investigated in much detail.<sup>6,9,10</sup> It was observed that exciton–photon coupling expressed as the longitudinal-transverse energy splitting is considerable stronger than in other II–VI or III–V semiconductors.<sup>11,12</sup> In ZnO nanostructures, exciton–photon coupling can even be considerably enhanced due to photon confinement.<sup>8</sup> For instance, in single ZnO nanowires a very large splitting of about 100 meV was observed between the upper and lower polariton branch.<sup>13</sup> Furthermore, the emission spectrum is characterized by marked Fabry-Pérot modes far below the band gap of ZnO (3.3 eV at room temperature) originating from strong exciton–photon coupling, not defects.<sup>14</sup>

Notwithstanding the strong interest of ZnO nanowires for nanophotonics and quantum optics, the microscopic (crystal-

lographic) origin of the luminescence and lasing in the wire geometry has not been discussed so far. Wurtzite ZnO has a complex valence band structure resulting in A, B, and C exciton transitions with well-defined transition dipoles with respect to the polar *c*-axis;<sup>10</sup> the A and B excitons have a preferential orientation perpendicular to the *c*-axis. The ZnO wires studied here are grown at high temperature (920 °C) and are chemically pure and highly crystalline. Such wires should be free of strain and hence represent a nearly ideal wurtzite lattice with the polar *c*-axis along the long axis of the wire. The diameter of the wires is above 100 nm implying that the optical properties are determined by an interplay of the crystalline structure with a complex electromagnetic mode structure.<sup>15,16</sup> In contrast to elongated semiconductor nanorods,<sup>17,18</sup> that are much smaller and hence have polarization properties that are entirely explained by electrostatic arguments for the polarizability of anisotropic scatterers, ZnO nanowires support several waveguide modes. Each of these modes has a complex polarized spatial mode structure across the wire. It is an intriguing question how the exciton transition dipoles with their specific orientation relative to the nanowire axis are coupled to the polarized electromagnetic waveguide modes of the ZnO nanowires. Understanding the polarization and microscopic origin of the different emission regimes of ZnO nanowires is furthermore of crucial importance for integration of ZnO nanowires as subwavelength waveguides and sources in nanophotonic circuits.

\* To whom correspondence should be addressed.

<sup>†</sup> University of Utrecht.

<sup>‡</sup> FOM Institute for Atomic and Molecular Physics (AMOLF).

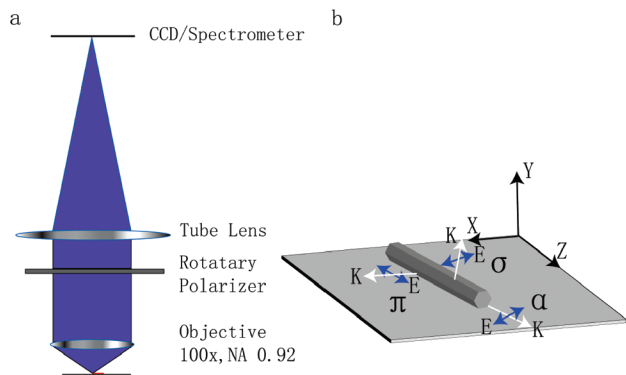


**Figure 1.** Set up and nomenclature for polarized luminescence measurements from a ZnO nanowire lying on a silica substrate. (a) Scheme of the luminescence microscope with a UV transparent objective with numerical aperture of 0.92 and collection angle of about 135°. A linear polarizer is placed between infinity corrected objective and tube lens. (b) Scheme of the emission modes using the conventional nomenclature, i.e.  $\alpha$  ( $\mathbf{k}/c$ ,  $\mathbf{E}\perp c$ ),  $\pi$  ( $\mathbf{k}\perp c$ ,  $\mathbf{E}/c$ ), and  $\sigma$ -emission ( $\mathbf{k}\perp c$ ,  $\mathbf{E}\perp c$ ). The relation between the degree of polarization observed at the polarizer behind the objective and the polarization of emission at the sample is summarized in Table 1.

Here, we present a polarization study of luminescence and lasing from single ZnO nanowires with diameters  $>100$  nm over the entire spectral region covering the visible and the near UV. This study combined with earlier results of spatially resolved emission shows that there are three distinct emission regimes. Besides the defect luminescence polarized along the wire ( $\mathbf{E}/c$ ), there is a second regime below the band gap, in which the emission occurs at the wire-ends only. The perpendicular polarization ( $\mathbf{E}\perp c$ ) reflects strong coupling of mainly B-excitons with waveguide modes with  $\mathbf{k}/c$  that are trapped between the wire end facets. This observation is consistent with a fully vectorial solution to Maxwell's equations that shows two linear transversely polarized fundamental waveguide modes. The flattened dispersion of these modes indicates the existence of two transverse exciton-polariton modes due to hybridization of the waveguide modes with the B-excitons. A marked dip of the polarization at around the electronic band gap at 3.3 eV indicates a third regime without guided modes. Most importantly, lasing is observed in the exciton-polariton regime only.

ZnO wires were grown epitaxially on a sapphire substrate using a vapor–liquid–solid method at high temperature (960 °C) with gold droplets as a catalyst.<sup>1,3,13</sup> Alternatively, wires were grown at higher Zn vapor pressure without using a catalyst. The wires are single crystalline, the  $c$  axis being the long axis, and the sides were faceted; the length of the wires was between 2 and 20  $\mu\text{m}$ , the diameter between 100 and 600 nm. After growth, the wires were transferred to a

silica substrate by simple rubbing, in order to perform single-wire optical studies.

We have studied the polarization of the emitted light in the entire visible and near UV region with a luminescence microscope (Zeiss, Axioplan 2) using an objective (Zeiss, EC Epiplan-Neofluor 100 $\times$ ) and tube lens that are transparent for visible and near UV light. The luminescence microscope and the geometry of emission from a ZnO nanowire lying on a silica substrate are presented in Figure 1 in which we have employed the nomenclature that is conventionally used for macroscopic ZnO crystals.<sup>10</sup> Single wires are uniformly excited through the microscope with a pulsed Nd:YLF laser at 349 nm (10 ns pulse length, 1.6 kHz repetition rate). The objective collecting the emitted light has a high numerical aperture of 0.92. The resulting large collection angle of 135° means that also a part of the light emitted with the wave vector nearly parallel to the  $c$ -axis (i.e.,  $\alpha$ -emission, see Figure 1b) can be collected. A detailed analysis of the collection of the polarization of the emitted light using a rotary linear polarizer placed in the parallel beam behind the objective is discussed in Supporting Information. In Table 1, we present the main conclusions of this analysis, which takes into account how polarization is transformed by refraction in the microscope objective. It is found that for emission modes with wave vector perpendicular to the wires long axis, that is, emission close to the optical axis of the microscope, both the  $\mathbf{E}/c$  and  $\mathbf{E}\perp c$  polarizations are retained behind the objective; this means that the  $\sigma$  and  $\pi$  polarization can be faithfully detected. More surprising are the results for light emitted almost along the long axis ( $\mathbf{k}/c$ ) of the wire, which enters the objective very far from the optical axis. It is clear a priori that this light ( $\alpha$ -polarization) is polarized perpendicular to the wire, due to transversality of electromagnetic waves. However, the  $\alpha$ -emission can still have any arbitrary polarization around the wire axis. Our analysis shows that isotropic polarization of emission around the wire axis translates into an isotropic detected polarization. Hence, any observed degree of polarization corresponds to a preferential polarization of the emission relative to the silica substrate. More explicitly, the  $\alpha$ -emission polarized perpendicular to the wire and along the substrate is faithfully detected with the polarizer aligned perpendicular to the wire. In contrast,  $\alpha$ -emission polarized perpendicular to both the wire and the substrate contributes to the collected signal with the polarizer parallel to the wire. Hence the overall intensity of the collected light with the polarizer aligned parallel to the wire is composed of a faithful  $\mathbf{E}/c$  emission at small emission angles ( $\mathbf{k}\perp c$  and  $\mathbf{E}/c$ ) and a “false” component originating from large emission angles ( $\mathbf{k}/c$ ,  $\mathbf{E}\perp c$ ). We conclude that the degree of detected polarization defined here as  $p(h\nu) = [(I_{P\perp c} - I_{P//c}) / (I_{P\perp c} + I_{P//c})]$  ( $I_{P\perp c}$ ,  $I_{P//c}$  collected

**Table 1.** Conversion Characteristics for Polarized, Directed Emission from a ZnO Nanowire Lying on a Flat Surface As Detected with a Luminescence Microscope As Sketched in Figure 1 with a Polarizer Behind the Objective

k-vector vs long axis (c)	polarization	name	detection by polarizer behind objective lens	coupling with excitons
$\mathbf{k}\perp c$	$\mathbf{E}\perp c$	$\sigma$	faithful	A, B
$\mathbf{k}\perp c$	$\mathbf{E}/c$	$\pi$	faithful	C
$\mathbf{k}/c$	$\mathbf{E}\perp c$ , parallel to substrate	$\alpha$	faithful	A, B
	$\mathbf{E}\perp c$ , perpendicular to substrate	$\alpha$	detected as parallel polarization	A, B

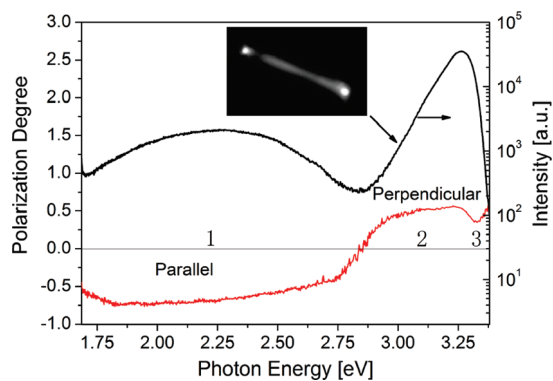


**Figure 2.** Spectrum (black) and degree of polarization (red),  $p(h\nu) = (I_{P\perp c} - I_{P\parallel c}) / (I_{P\perp c} + I_{P\parallel c})$ , of the emission from a ZnO nanowire (250 nm in diameter and 12  $\mu\text{m}$  in length), lying on a silica substrate. The three emission regimes discussed in the text are indicated with 1, 2, 3. In regime 1, light is emitted uniformly over the entire wire and polarized parallel to the wire. In the second regime, light is emitted at the wire ends only (see insert of spatial emission of the wire) and polarized perpendicular to the wire axis, in plane with the substrate. The marked dip in the polarization at the bandgap indicates the third regime.

intensity with polarizer aligned perpendicular and parallel to the wire, respectively) is a good measure of  $\sigma$  and  $\pi$  polarization and furthermore quantifies the amount of in-plane polarization within the  $\alpha$ -emission. Of course, this analysis is specific for wires lying flat on the silica substrate. We have also performed reference measurements with wires that stand up vertically and under an angle with the substrate. For instance, in the vertical geometry the  $\alpha$ -polarization should consist of light emitted perpendicular to the substrate plane with the  $\mathbf{E}$  vector isotropically distributed in the plane of the substrate and with wave vector pointing along the optical axis of the microscope. Experimentally we indeed retrieved isotropic emission in this case, consistent with our analysis.

We have measured the emission spectrum and the degree of polarization of tens of ZnO nanowires of varying diameter (100–600 nm) and length (2–20  $\mu\text{m}$ ) lying on a flat silica substrate. Figure 2 shows a typical example; the emission spectrum shows a broad defect luminescence between 1.75 and about 2.9 eV, and a second band with blue and near UV luminescence below and at the band gap of ZnO (3.3 eV at room temperature). We remark that the ratio of the defect and near UV emission intensities depends on the excitation intensity; the latter completely dominates at increasing intensity. The defect luminescence is strongly polarized parallel to the wire axis, that is,  $\mathbf{E}\parallel c$ . Strikingly, the polarization switches abruptly from mainly parallel ( $\mathbf{E}\parallel c$ ) into mainly perpendicular to the wire's long axis ( $\mathbf{E}\perp c$ ) at around 2.9 eV; the perpendicular polarization parallel to the substrate plane is retained up to a photon energy of about 3.22 eV. There is a marked dip in the degree of polarization between 3.25 and 3.35 eV, indicative for another regime of light emission. These three regimes of emission are observed for all wires that we studied. The dip in the degree of polarization in the third region varies from wire to wire, but the minimum is often close to zero.

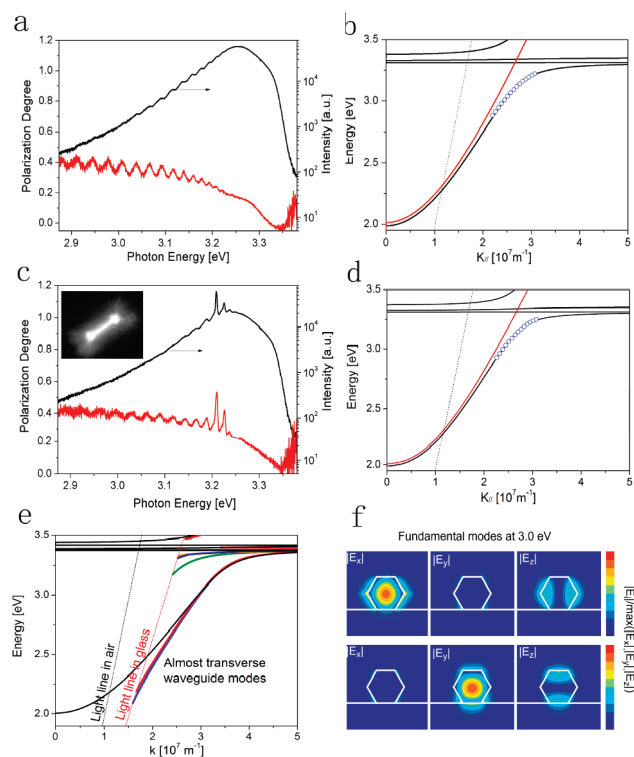


**Figure 3.** Spectra (black) and degree of polarization (red) of the emitted light from a single ZnO nanowire (170 nm in diameter, 5  $\mu\text{m}$  in length) in the region between 2.9 and 3.4 eV and the corresponding dispersion relation. (a) Low excitation intensity. The emission spectrum consists of a series of Fabry-Pérot luminescence modes between 2.9 and 3.22 eV that are also observed in the degree of polarization. (b) The Fabry-Pérot maxima plotted in the energy-wave vector diagram and fitted with the classical polariton equation. (c,d) As a,b but at higher excitation intensity. Some of the modes develop into sharp lasing peaks, the dispersion relation remains strongly curved. The inset in c shows the lasing nanowire with typical interference pattern. (e) The exact dispersion relations for fundamental and higher order modes together with the classical dispersion relation  $\varepsilon(\omega)\omega^2/c^2 = k^2 + 2\pi^2/d^2$  (black curve) where  $\varepsilon(\omega)$  contains the A, B, C excitons, and where  $d$  is the wire diameter. Dashed lines: light lines in air and glass. Color curves: exact dispersion (hexagonal side of wire 86 nm) for the fundamental modes (blue, red) and higher order modes (beyond 3.2 eV). (f) Contour plots of  $|\mathbf{E}_x|$  ( $\mathbf{E}$ -field along the substrate),  $|\mathbf{E}_y|$  (perpendicular to the substrate) and  $|\mathbf{E}_z|$  (along the wire) for the two fundamental modes at 3.0 eV. Color scales for each mode are normalized to  $\max(|\mathbf{E}_x|, |\mathbf{E}_y|, |\mathbf{E}_z|)$ .

We now correlate these results with those of a spatially resolved luminescence spectroscopy reported in a previous study.<sup>14</sup> This study showed that emission in the first regime (1.75–2.9 eV) was emitted uniformly over the length of the wire, while in the second regime (2.9 – 3.22 eV) light is emitted at the wire ends only (see insert of Figure 2). Since  $\mathbf{k}\parallel c$ , and  $\mathbf{E}\perp c$ , the emission that we detect in regime 2 corresponds to the  $\alpha$ -emission in conventional nomenclature. Note that the observed degree of polarization implies emission preferentially polarized along the substrate. The wire that we present in Figure 2 has a length of 12  $\mu\text{m}$ . Shorter wires show pronounced Fabry-Pérot resonances in their emission spectrum, that allow us to characterize the second emission regime in more detail. Figure 3 shows emission and polarization spectra of a wire of 5  $\mu\text{m}$  in length

and 170 nm in diameter, uniformly excited with 349 nm light with low and higher intensity. In addition to the Fabry-Pérot peaks in the emission spectrum, the degree of polarization also shows a series of Fabry-Pérot peaks. The resonances observed in the degree of polarization correspond unambiguously to the resonances observed in the emission spectrum. The fact that the Fabry-Pérot modes are so clearly seen in the degree of polarization versus energy plot points to an unpolarized background emission occurring together with the polarized polariton modes. Since, ideally the polariton modes (with  $\mathbf{k} \parallel c$  and  $\mathbf{E}$  perpendicular to  $c$ ) have a Lorentzian frequency spectrum of limited width (defined by the quality factor of the nanowire cavity), the degree of polarization peaks at each resonance energy, and decreases to reach a minimum set by the background between two resonances. A plot of these “polarization resonances” in the energy-wave vector diagram shows strong curvature and deviation from the light line, typical for strong exciton-photon coupling (vide infra).

We first address the microscopic origin of the first and second emission regime. We observed that the defect emission (first regime) is strongly polarized with  $\mathbf{E} \parallel c$ . Given that this emission has  $\mathbf{k} \perp c$ , it corresponds to  $\pi$ -emission. This points to a recombination process in which the C-type valence band is involved; hence, a trapped electron should recombine with a hole in the C-valence band (split-off band). The mechanism agrees with previous results obtained with ZnO quantum dots that proved, on account of quantum confinement, that the defect luminescence is due to an electron trapped in a localized state (very probably an oxygen vacancy) recombining with a valence band hole.<sup>19</sup> We remark here that with a wire that is tilted with respect to the substrate plane, the green emission shows Fabry-Pérot resonances that are equidistant in energy (see Supporting Information, Figure S2). These resonances retain the  $\mathbf{E} \parallel c$  polarization as opposed to the  $\mathbf{E} \perp c$  resonances in the second regime. This observation points to coupling of the defect luminescence with longitudinal components of the waveguide modes. From our finite element analysis of Maxwell's equations,<sup>20</sup> ZnO nanowires of sufficient thickness can indeed sustain waveguide modes with large longitudinal ( $\mathbf{E} \parallel c$ ) field components. In addition, even the fundamental modes already provide a longitudinal component away from the center of the wire (Figure 3f).

With regard to the microscopic origin of the third regime, roughly between 3.25 and 3.35 eV, we recall from Figure 2 that it is characterized by a sharp “dip” in the degree of polarization, which can be interpreted as due to a luminescence contribution with mainly  $\mathbf{E} \parallel c$  polarization. The previous observation that above 3.22 eV, emission occurs abruptly over the entire wire (in contrast to below 3.22 eV) shows that the emission is not exclusively due to modes strongly confined between the wire ends. We note that there are several possible origins of this contribution. As a first possibility, mixed modes based on A and B excitons have been put forward for the case of macroscopic ZnO. Our mode analysis provides support for this mechanism, since we find a plethora of higher order complex modes. These higher modes are characterized by substantial  $\mathbf{E} \parallel c$  component near

the outside of the wire, as well as by the fact that they are only weakly confined ( $\mathbf{k}$  near the light line). As an alternative explanation, we note that the strong  $\pi$ -polarization together with the energetic position of the dip (blue shift by some tens of millielectronvolts with respect to the resonances in regime 2) provides an indication that the emission in the third regime is most probably related to the C exciton. This is in line with the interpretation of the strong resonance with  $\mathbf{E} \parallel c$  polarization blue shifted with respect to the A and B transitions observed for macroscopic ZnO crystals, which has been attributed to the C exciton that has a strong oscillator strength in the direction parallel to the  $c$ -axis (for a review, see ref 1).

The emission between 2.9 and 3.22 eV is not classic in any sense, since it consists of eigenmodes trapped between the end-facets of the wire of energy considerably below the electronic band gap. The  $\mathbf{E} \perp c$  polarization that we observe in this region, that is,  $\alpha$  polarization,<sup>1,10</sup> agrees with the picture of delocalized exciton-polaritons; A and B excitons with allowed transition dipoles that have  $\mathbf{E} \perp c$  can maximally couple with the two almost degenerate fundamental waveguide modes of the wire, which have almost transverse linearly polarized mode profiles (Figure 3f). We remark that we detect a clear preference for polarization parallel to the substrate plane. This is consistent with the observations in ref 4 and the explanation therein that modes polarized perpendicular to the SiO<sub>2</sub> substrate plane are preferentially outcoupled into the substrate and hence missed in the collection<sup>4</sup> from the air side. The longitudinal-transverse splitting of the A and B excitons is 1.45 and 5 meV, respectively;<sup>1</sup> hence we must conclude that the strong exciton-photon coupling that we observe is mainly related to the B exciton. On the basis of the Fabry-Pérot maxima in the polarization spectrum, which are better resolved than the correlated maxima in emission intensity, we have determined the  $\mathbf{E}, \mathbf{k}$  dispersion diagrams (Figure 3b,d), which we can compare with the classical exciton-polariton dispersion. The dispersion plot becomes increasingly curved with increasing energy toward the B exciton line and can be well fitted with the classic exciton-polariton dispersion equation, under the condition that B exciton-photon coupling is assumed to be 5 times stronger than for bulk ZnO.

The classical exciton polariton dispersion equation is derived under the simplified condition that the wire acts as a guide of square cross section with perfectly conducting boundaries, implying that the transverse mode profile has one maximum across the width of the wire, and goes to zero on the wire perimeter. In reality, the mode structure is more complex, as the vectorial modes can extend outside the wire, depending on the electromagnetic boundary conditions. We have undertaken a fully vectorial finite element waveguide dispersion calculation<sup>20</sup> for the hexagonal wires, including the silica substrate (Figure 3e). In this analysis, we assume a wire with a hexagonal side (length 86 nm, leading to a diameter of approximately 170 nm) lying on a flat glass substrate ( $n = 1.5$ ) and surrounded by air. The finite element solver solves the wave equation for the transverse components of the H-field (from which all other field components

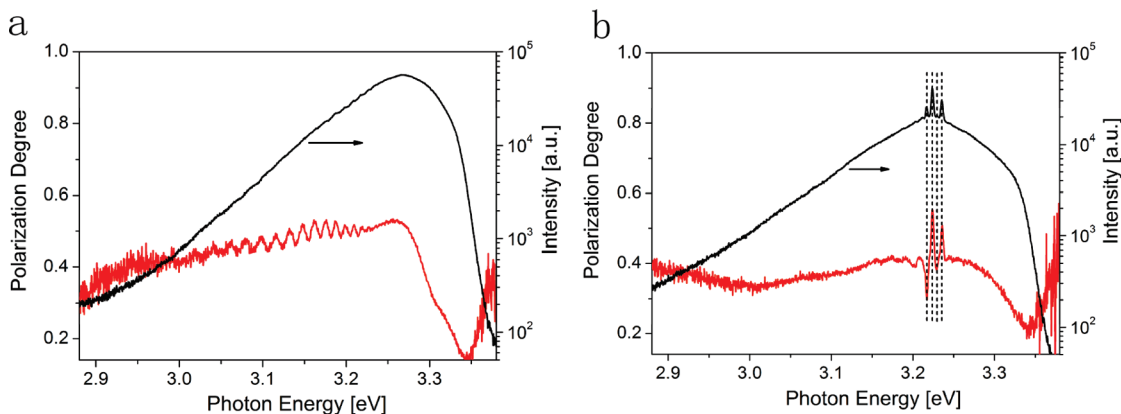


**Figure 4.** Spectra (black) and polarization (red) of the emitted light from a single ZnO nanowire (600 nm in diameter, 6.7  $\mu\text{m}$  in length) at low and high excitation intensity. (a) Low excitation intensity. The emission spectrum consists of a series of Fabry–Pérot luminescence modes between 2.9 and 3.22 eV also reflected in the degree of polarization. (b) At higher excitation intensity, sharp laser peaks arise at around 3.2 eV, the two laser peaks at the highest energy have  $\mathbf{E}\perp\mathbf{c}$  polarization, the third laser peak has a  $\mathbf{E}\parallel\mathbf{c}$  polarization.

are calculated) on a grid with a grid spacing of 0.5 nm in and near the wire. The grid coarsens toward the edge of the simulation domain ( $3\lambda$  away from the wire), where we impose zero-field boundary conditions. The dielectric response of the wire is described exactly as in the case of the classical exciton-polariton dispersion relation (i.e., with exciton–photon coupling for the B-exciton 5-fold enhanced compared to bulk ZnO). The hexagonal wires support two fundamental modes that start at the light line in glass at around 2.2 eV. The dispersion curve is fully consistent with the classical exciton-polariton dispersion in the energy range above  $\sim 2.75$  eV. The corresponding waveguide modes are not strictly transverse electric (TE) or transverse magnetic modes (TM), but are of hybrid nature, as in the case of cylindrical waveguides. Mode profiles for the electric field in Figure 3f demonstrate that these modes can effectively be viewed as TE-like, since aside from a weak longitudinal field component along the wire, these modes are dominantly linearly polarized orthogonal to the wire. A slight splitting between the modes is due to a perturbative effect of the substrate and the orientation of the polarization relative to the hexagonal cross section. We conclude that the full dispersion relation for these almost transverse, linearly polarized electric modes fit the experimental Fabry–Pérot resonances very well, indicating that the resonances are due to B-excitons hybridizing with the fundamental waveguide modes to form almost transverse exciton-polaritons. It should be remarked that besides the fundamental linearly polarized modes, Maxwell’s equations lead also to several other modes, often with a complex polarization, that have a cutoff at higher energies of around 3.2 eV for this particular wire diameter. The cutoff shifts to lower frequencies for thicker wires. It is possible that these modes are not observed experimentally, potentially because they cannot be sufficiently coupled to the B exciton due to a mismatch with the transition dipole moment and furthermore due to poor coupling into the collection optics. A more detailed study, preferably with access to the near-field, is required to resolve this issue.

At higher excitation intensities, one or several of the Fabry–Pérot resonances corresponding to guided B-exciton polari-

tons develop into sharp laser peaks at around 3.2 eV with a pronounced degree of perpendicular polarization; see Figure 3c. Another example is shown in Figure 4 (discussed below). We have studied the onset of lasing on 10 wires with different diameters and lengths. Strikingly, the lasing peaks always develop at around 3.2 eV, and were never observed at the electronic band gap (3.3 eV). The dispersion curve of the Fabry–Pérot modes (as determined from the polarization resonances) at this excitation intensity remains strongly curved, and fits the exciton-polariton dispersion curve (Figure 3d). This indicates that strong coupling between B excitons and the linearly polarized transverse electric modes lies at the origin of lasing. Hence, room-temperature lasing is mediated by the fundamental exciton-polariton modes of the wire.

In the case of ZnO nanowires with a larger diameter, laser peaks with orthogonal polarization can coexist. Figure 4 presents emission and polarization spectra of a ZnO nanowire with a diameter of 600 nm. As for thinner ZnO wires, laser peaks again develop at around 3.2 eV. However, besides the commonly observed  $\mathbf{E}\perp\mathbf{c}$  polarization, one laser peak has  $\mathbf{E}\parallel\mathbf{c}$  polarization. In simple language, the lasing with  $\mathbf{E}\parallel\mathbf{c}$  can be assigned to higher order modes with higher azimuthal quantum number (i.e., whispering gallery-like modes), which are also evident in our waveguide mode analysis (results not shown). For these thicker wires, our solutions to Maxwell’s equations lead to a plethora of waveguide modes, often with a complex polarization. The above result shows that at least one of these modes can compete successfully for gain with the commonly observed transverse electric modes.

In summary, we have measured the degree of polarization of the light emitted from single ZnO nanowires. We have observed three distinct polarization regimes that also correspond to distinct modes of emission. In the intermediate regime, below the electronic bandgap of ZnO, the degree of polarization shows Fabry–Pérot type peaks with an enhanced polarization perpendicular to the wires long axis. These results show that there is a strong interaction between the B-exciton and transverse, linearly polarized modes trapped between the end facets of the wire, that is, strong

exciton–photon coupling. At higher excitation intensity, one or more of these exciton–polariton modes evolves into a sharp laser peak.

**Acknowledgment.** This work is part of the research program of the “Stichting voor Fundamenteel Onderzoek der Materie” (FOM), which is financially supported by the “Nederlandse Organisatie voor Wetenschappelijk Onderzoek” (NWO). A.F.K. furthermore acknowledges a VENI fellowship funded by NWO, and “NanoNed”, a nanotechnology program funded by the Dutch Ministry of Economic Affairs. H.-Y.L. acknowledges the support from NWO-CW, Topgrant 700.53.308 and NanoNed.

**Supporting Information Available:** This material is available free of charge via the Internet at <http://pubs.acs.org>.

## References

- (1) Ozgur, U.; Alivov, Y. I.; Liu, C.; Teke, A.; Reshchikov, M. A.; Dogan, S.; Avrutin, V.; Cho, S. J.; Morkoc, H. *J. Appl. Phys.* **2005**, *98*, 041301.
- (2) Djurisic, A. B.; Leung, Y. H. *Small* **2006**, *2*, 944.
- (3) Huang, M. H.; Mao, S.; Feick, H.; Yan, H.; Wu, Y.; Kind, H.; Weber, E.; Russo, R.; Yang, P. *Science* **2001**, *292*, 1897.
- (4) Johnson, J. C.; Yan, H. Q.; Yang, P. D.; Saykally, R. J. *J. Phys. Chem. B* **2003**, *107*, 8816.
- (5) Law, M.; Sirbuly, D. J.; Johnson, J. C.; Goldberger, J.; Saykally, R. J.; Yang, P. *Science* **2004**, *305*, 1269.

- (6) Thomas, D. G. *J. Phys. Chem. Solids* **1960**, *15*, 86.
- (7) Gil, B.; Kavokin, A. V. *Appl. Phys. Lett.* **2002**, *81*, 748.
- (8) Zamfirescu, M.; Kavokin, A.; Gil, B.; Malpuech, G.; Kaliteevski, M. *Phys. Rev. B* **2002**, *65*, 161205.
- (9) Schmidt-Grund, R.; Rheinlander, B.; Czekalla, C.; Benndorf, G.; Hochmuth, H.; Lorenz, M.; Grundmann, M. *Appl. Phys. B* **2008**, *93*, 331.
- (10) Toropov, A. A.; Nekrutkina, O. V.; Shubina, T. V.; Gruber, T.; Kirchner, C.; Waag, A.; Karlsson, K. F.; Holtz, P. O.; Monemar, B. *Phys. Rev. B* **2004**, *69*, 165205.
- (11) Lagois, J. *Phys. Rev. B* **1981**, *23*, 5511.
- (12) Chichibu, S. F.; Sota, T.; Cantwell, G.; Eason, D. B.; Litton, C. W. *J. Appl. Phys.* **2003**, *93*, 756.
- (13) van Vugt, L. K.; Rühle, S.; Ravindran, P.; Gerritsen, H. C.; Kuipers, L.; Vanmaekelbergh, D. *Phys. Rev. Lett.* **2006**, *97*, 147401.
- (14) Rühle, S.; van Vugt, L. K.; Li, H. Y.; Keizer, N. A.; Kuipers, L.; Vanmaekelbergh, D. *Nano Lett.* **2008**, *8*, 119.
- (15) Maslov, A. V.; Ning, C. Z. *Appl. Phys. Lett.* **2003**, *83*, 1237.
- (16) van Vugt, L. K.; Zhang, B.; Piccione, B.; Spector, A. A.; Agarwal, R. *Nano Lett.* **2009**, *9*, 1684.
- (17) Hu, J.; Li, L.-S.; Yang, W.; Manna, L.; Wang, L.-W.; Alivisatos, A. P. *Science* **2001**, *292*, 2060.
- (18) Wang, J.; Gudixsen, M. S.; Duan, X.; Cui, Y.; Lieber, C. M. *Science* **2001**, *293*, 1455. (2001).
- (19) Dijken, A. v.; Meulenkaamp, E. A.; Vanmaekelbergh, D.; Meijerink, A. *J. Lumin.* **2000**, *90*, 123.
- (20) Fallahkhair, A. B.; Li, K. S.; Murphy, T. E. *J. Lightwave Technol.* **2008**, *26*, 1423.

NL9017012